


Comparison of round and knife-edge-like cathodes on gas-puff implosions

J. C. Valenzuela ^{*}, M. Escalona , O. Loch , F. Veloso , and J. P. Díaz 
Pontificia Universidad Catolica de Chile, Santiago 7820436, Chile

 (Received 14 February 2023; accepted 27 June 2023; published 9 August 2023)

Preionization is believed to play an important role on the implosion of gas-puff Z pinches. Some experiments have used an external preionization source, e.g., UV light or electron beam. In contrast, other experiments rely completely on over voltage breakdown by the own generator's voltage pulse. However, this approach lacks shot-to-shot reproducibility since self-breakdown is mainly a stochastic process. In this work, we performed a systematic study on self-breakdown using two different cathode geometries: (i) a smooth, round cathode to provide a homogeneous electric field, (ii) a sharp, knife-edge-like geometry to enhance the electric field locally and eventually electron emission. The experiments were carried out on the Llampudken current generator, which provides a current pulse of ~ 400 kA amplitude and 200 ns rise time (10%-90%). We implemented gated XUV imaging, filtered diodes and time-integrated x-ray imaging to obtain information about the implosion as well as the stagnation phase for the two cathode geometries. We found that erosion of the knife-edge cathode might be a serious problem, and we had to replace it every 15 shots. On the other hand, the round cathode lasted for the whole series of experiments. We also measured a more reproducible and larger peak current for the knife cathode. From the photo-conductive detectors we observed that even if the round cathode might present shots with higher x-ray yield compared to the knife cathode, dispersion is almost twice as large. Moreover, after a statistic analysis, it is demonstrated that the dispersion in the yield is due solely to differences imposed by the cathodes and not to variations in the driver, as no correlation was found between them. We found that in order to fit the experimental data with the snowplow model, only $\sim 60\%$ of the total mass is compressed in the knife cathode while $\sim 20\%$ for the round one, highlighting the importance of the cathode and preionization. Therefore, we conclude that the use of the knife cathode increases the reproducibility of the experiment in comparison with the round cathode.

DOI: [10.1103/PhysRevE.108.025202](https://doi.org/10.1103/PhysRevE.108.025202)

I. INTRODUCTION

Gas-puff Z pinches have been studied for more than three decades as a way to produce high energy density plasmas using pulsed power with main applications to radiation sources [1,2] and fusion studies [3,4]. In a gaspuff, a fast electromagnetic valve opens quickly to inject gas into the anode-cathode gap of a pulsed power generator [5–7]. Then, the current pulse heats and compresses the gas load to a small volume as consequence of the Lorentz force. One of the key features of gaspuffs is that the load can be injected repeatedly without changes in the hardware, as opposed to other pulsed power configurations, e.g., liners or wire arrays, making it attractive for applications which require a high repetition rate.

Most of the gas-puff experiments have mainly concentrated on the final stages of the pinch, i.e., implosion and stagnation [8]. Nevertheless the early phase is important as well. For instance, it influences the development of magneto-Rayleigh-Taylor instability since its amplitude at time t ($A(t)$) is proportional to the initial amplitude: $A(t) = A_0 e^{\Gamma t}$, here A_0 is the initial perturbation amplitude and Γ is the growth rate—for incompressible fluids $\Gamma = \sqrt{gk}$, where g is the sheath acceleration and k is the wave vector of the instability.

Therefore, if the initial amplitude can be reduced in the early phase, then the quality of the implosion and stagnation phases can be improved, reaching higher final pressures before pinch disruption.

The neutral gas, initially injected by the nozzle, has to become a good electrical conductor to conduct the generator's current and subsequently implode and pinch. The initial gas ionization (which we call preionization from now on) can happen in several ways. The more obvious case is the self-breakdown case when the driver's voltage is applied, which has to exceed the Paschen minimum along some trajectory between the anode and cathode electrode. Many current drivers have a voltage prepulse that precedes the main driving pulse. If the prepulse is sufficiently high, the gas could breakdown and conduct its current, resulting in gas preionization. Then, a current path has been established for the main current pulse. Another way to preionize the gas is to use an external process, for example ultraviolet (UV) [9,10] radiation or an electron beam [11]. In this way, a reproducible current path could be established before the current pulse arrives.

Regardless of how the preionization is done, a consistent and uniform current path is beneficial for experimental reproducibility and pinch symmetry. Shot-to-shot reproducibility is a highly desired feature for both, scientific and application points of view. Asymmetry, on the other hand, can limit the pinch compression to a large radius, reducing the achievable

^{*}jvalenzuela@fis.uc.cl

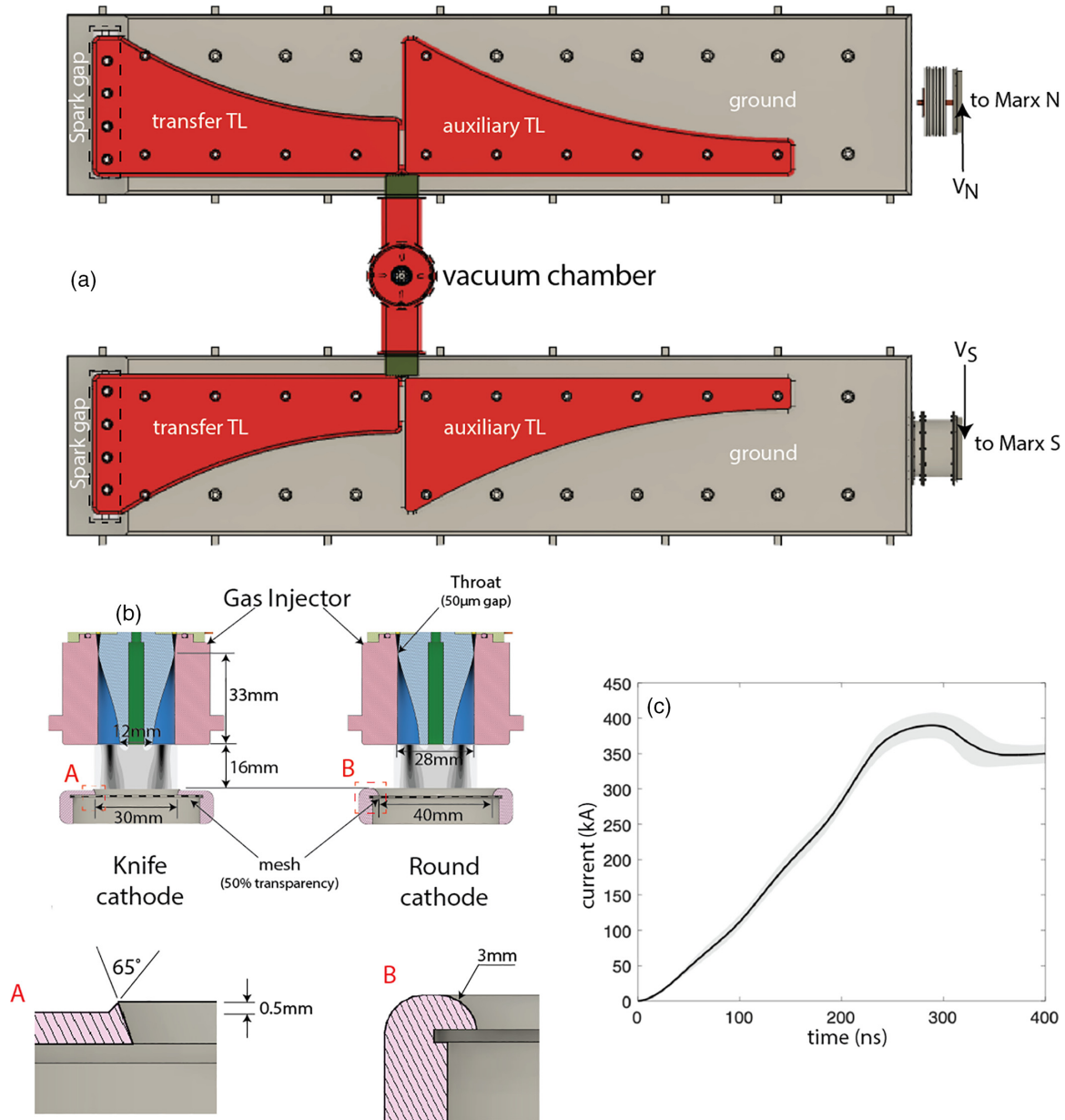


FIG. 1. (a) Llampuden drawing showing the transmission lines and vacuum chamber. Exponential transfer lines are used for impedance matching. (b) Gas injector produces a hollow gas column, two types of cathodes were implemented: knife and round. (c) Ten-shot current average using a gas-puff load.

density and temperature of the pinch. Furthermore, knowing the initial current path would be beneficial for understanding experimental results as well as to initialize simulations.

The breakdown process by itself is statistical, depends on the details of the injected gas and generator characteristics, and can lead to individual current carrying channels thereby imprinting azimuthal nonuniformities and unstable filamentary structures at an early stage of the discharge. For a high-current generator that relies on the prepulse or high dI/dt to initiate the gas breakdown, the radius at which the breakdown occurs will depend on the Paschen minimum for the particular gaspuff and on generator parameters. When large, structured profiles are used, the radius at which the implosion begins might not be the nominal radius of the nozzle and might vary with axial location. Furthermore, it

is not clear whether this would be beneficial for the gas-puff implosion, because during the long prepulse numerous ionization-radiation instabilities could develop and lead to strong perturbation of the initial state [12].

In general, there are indications that preionization contributes to the stability of the implosion, the reproducibility of the compression, and an increase in the total K-shell yield at stagnation. However, no systematic studies of the effect of preionization have been performed and the question of whether or not preionization is helpful for improving the quality of implosions remains somewhat open.

In this work, we perform a systematic study on the effect of the cathode geometry on self-breakdown of single liner gaspuff and how it affects the implosion and stagnation dynamics.

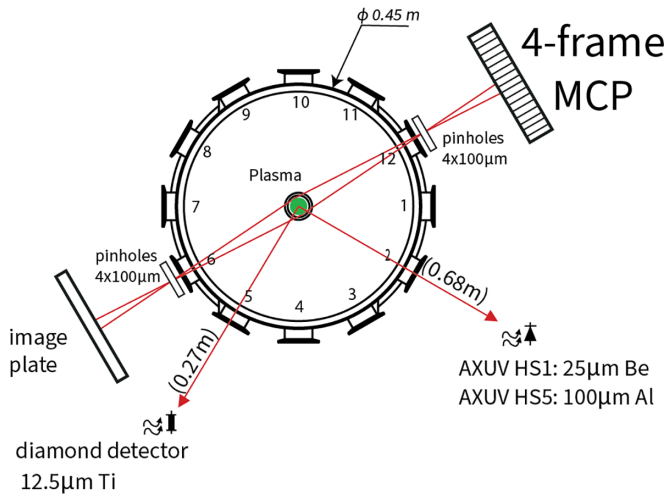


FIG. 2. Top view of Llampudken’s vacuum chamber showing the diagnostics implemented in this work. A gated XUV camera was implemented on port 12, enabling the detection of four images from a single shot. Radiation detectors were installed on ports two and five to measure x-ray emission as a function of time. Additionally, a time-integrated pinhole camera with matching filters to the radiation detectors was mounted on port six.

II. EXPERIMENTAL CONFIGURATION

The experiment was carried out on the Llampudken pulsed power generator. Llampudken uses exponential transmission lines (TL) for a better impedance match between the principal

transmission line and the load, as well as auxiliary transmission lines connected in parallel to the load section. As Fig. 1(a) shows, Llampudken consists of two Marx generators driving a set of transmission lines connected in parallel to the load (we call them north and south). Each Marx comprises of 12 capacitors of 3 μF each which are normally charged to 22 kV (40 kV maximum voltage) producing a ~1 μs voltage pulse that charges a parallel plate transmission line (STL), which is located under the gray ground plate in Fig. 1(a). When fully charged, the fourchannel sparkgap (SG) is triggered and the STL is discharged into the load through the exponential transfer TL. The auxiliary TL controls the voltage at the load and allows energy to be reflected back at later times to the load when the other end is left open, increasing the overall energy coupling into the load [13]. A 10-shot current average wave form is shown in Fig. 1(c), we measured a peak current of ~400 kA in 200 ns rise time (10%-90%).

The load used in this work was a single argon liner gas-puff producing a mass per unit length of ~15 μg/cm ± 50%. The error corresponds to the uncertainty in the measurement and not necessarily the fluctuation in the density. Considering all the relevant parameters that affect the gas density, we estimate a variation in the density of less than 10%. This value does not explain the uncertainties found in current or x-ray yield.

The injector operated at 2.2 Bar (plenum) and Llampudken was fired 360 μs after the valve was opened, when the gas flow has almost reached a steady state. Gas density increases linearly with time from 180 μs to 400 μs. We used ANSYS Fluent to design the injector nozzle, which consisted of a de Laval-like nozzle opened by an electromagnetic valve, as

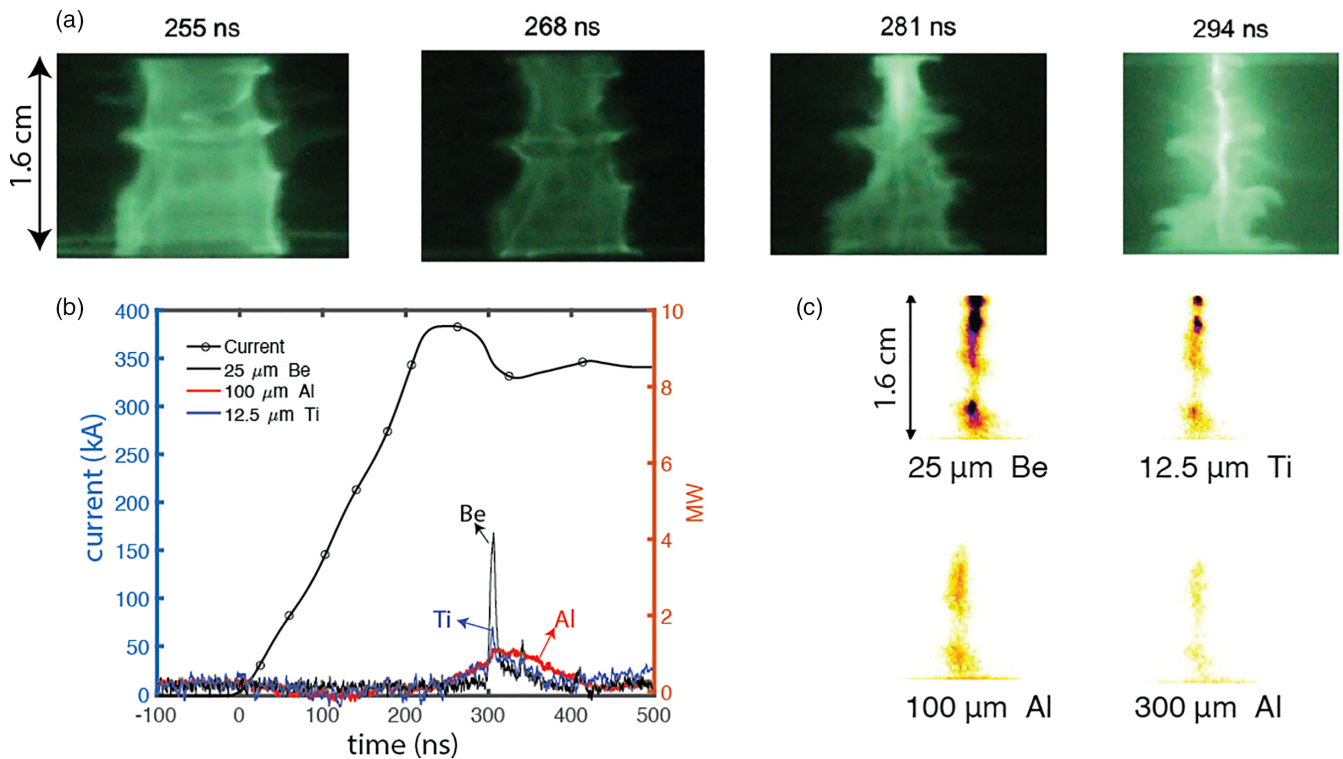


FIG. 3. (a) XUV imaging showing the gas-puff implosion for argon load. (b) Current and filtered photo-conductive detectors showing x-ray pulse obtained in the experiment. (c) X-ray time-integrated imaging obtained with filtered pinhole camera. We used the filters: 25 μm Be, 12.5 μm Ti, 100 μm Al, 300 μm Al.

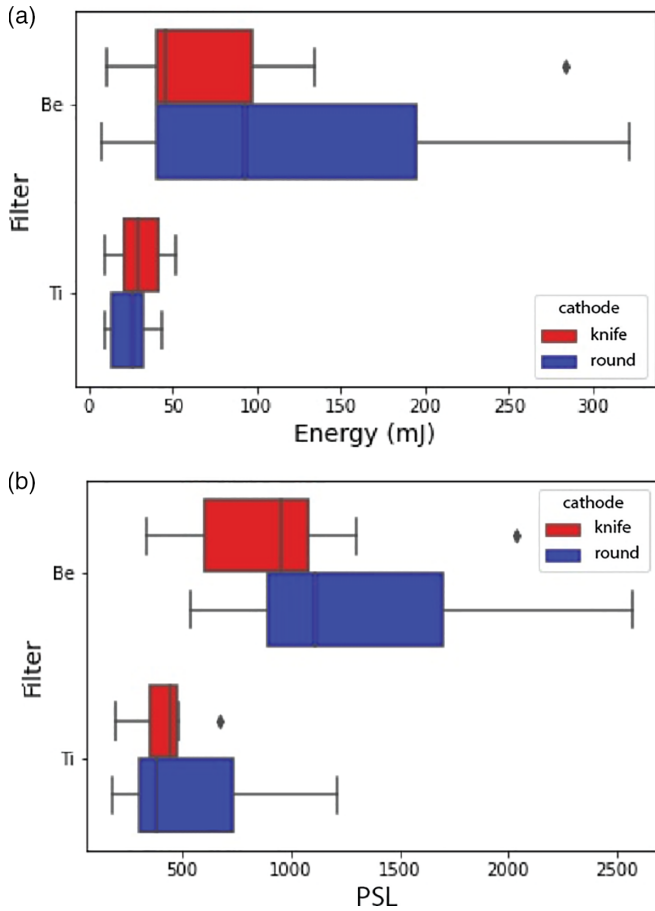


FIG. 4. X-ray yield for both cathodes obtained from (a) photoconductive detectors and (b) time integrated pinhole camera.

described in Ref. [14]. According to simulations, a supersonic ($M > 4$) gas column is produced at the injector exit preventing large gas expansion. This type of simulation has been extensively validated in other work, see for example Ref. [15].

To study reproducibility, we performed a systematic study on self-breakdown using two different cathode geometries: (i) a smooth, round cathode to provide a homogeneous electric field and (ii) a sharp, knife-edge-like geometry to enhance the electric field locally and eventually improve electron emission; both cathode geometries are shown in Fig. 1(b).

The initial gas column diameter is ~ 28 mm and both cathode diameters are designed to have a larger aperture to avoid gas reflection from the cathode. For the the knife cathode the aperture was 30 mm and at the edge it has a 65° protuberance with less than $50 \mu\text{m}$ initial radius. On the other hand, the round cathode aperture was 40 mm and it was rounded to 3 mm. Electromagnetic simulations using the code ANSYS Maxwell software show an increment of the local electric fields of at least a factor of $\times 3$ (not shown here). The knife cathode was designed so it is right at the edge of the gas column and it can have an effect on the the gas.

The plasma dynamics and x-ray yield were studied using a series of diagnostics that are shown in Fig. 2. In port 12 we implemented a time gated (4 ns) XUV imaging system to record self-emission of the plasma providing information about the compression and uniformity of the pinch. We do

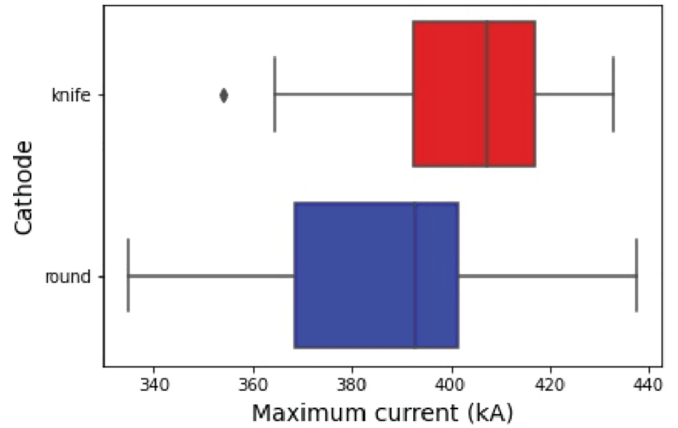


FIG. 5. Peak current for both cathodes. The median is larger for the knife cathode (407 kA) compared to the round one (393 kA), and it also shows less data dispersion.

not use any filters here and the sensitivity is given by the microchannel plate’s (MCP) photocathode, i.e., gold. Filtered diode on port two ($25 \mu\text{m}$ Be filter and $100 \mu\text{m}$ Al) and diamond detector on port five ($12.5 \mu\text{m}$ Ti filter) were used to measure x-ray yield. Finally, we used time-integrated x-ray pinhole images in different spectral regions using filters (port six). These images provide information about how homogeneous the final compression is and therefore, about pinch stability. The filters implemented were $25 \mu\text{m}$ Be, $12.5 \mu\text{m}$ Ti, $100 \mu\text{m}$ and $300 \mu\text{m}$ Al. The Be filter lets through emissions above ~ 1 keV, while the Ti filter records K-shell emission around 3 keV, and both Al filters, $100 \mu\text{m}$ and $300 \mu\text{m}$, record emission from >6 keV and >8 keV, respectively. To record the data we used BAS-MS image plate and the Fujifilm FLA-5100 scanner to read them.

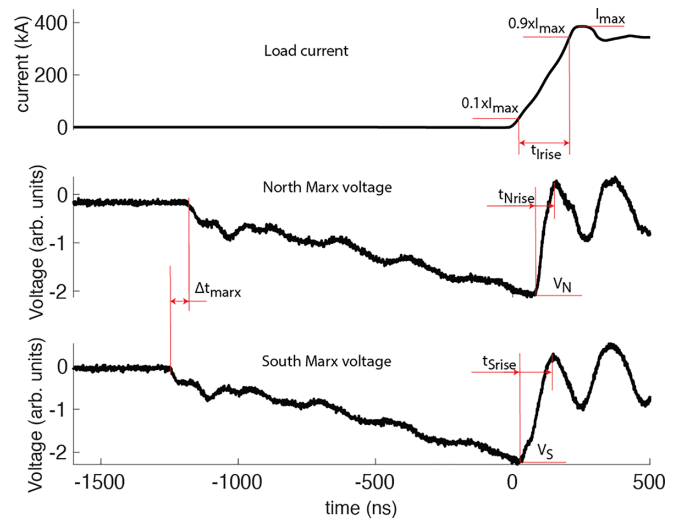


FIG. 6. At the top we show the current through the load and the definition of t_{rise} and I_{max} . Second and third plot, we show the Marx voltage and how we define the parameters Δt_{max} , V_N , V_S , $t_{N\text{rise}}$, $t_{S\text{rise}}$. We want to find if there is any correlation between any of these five parameters on the current.

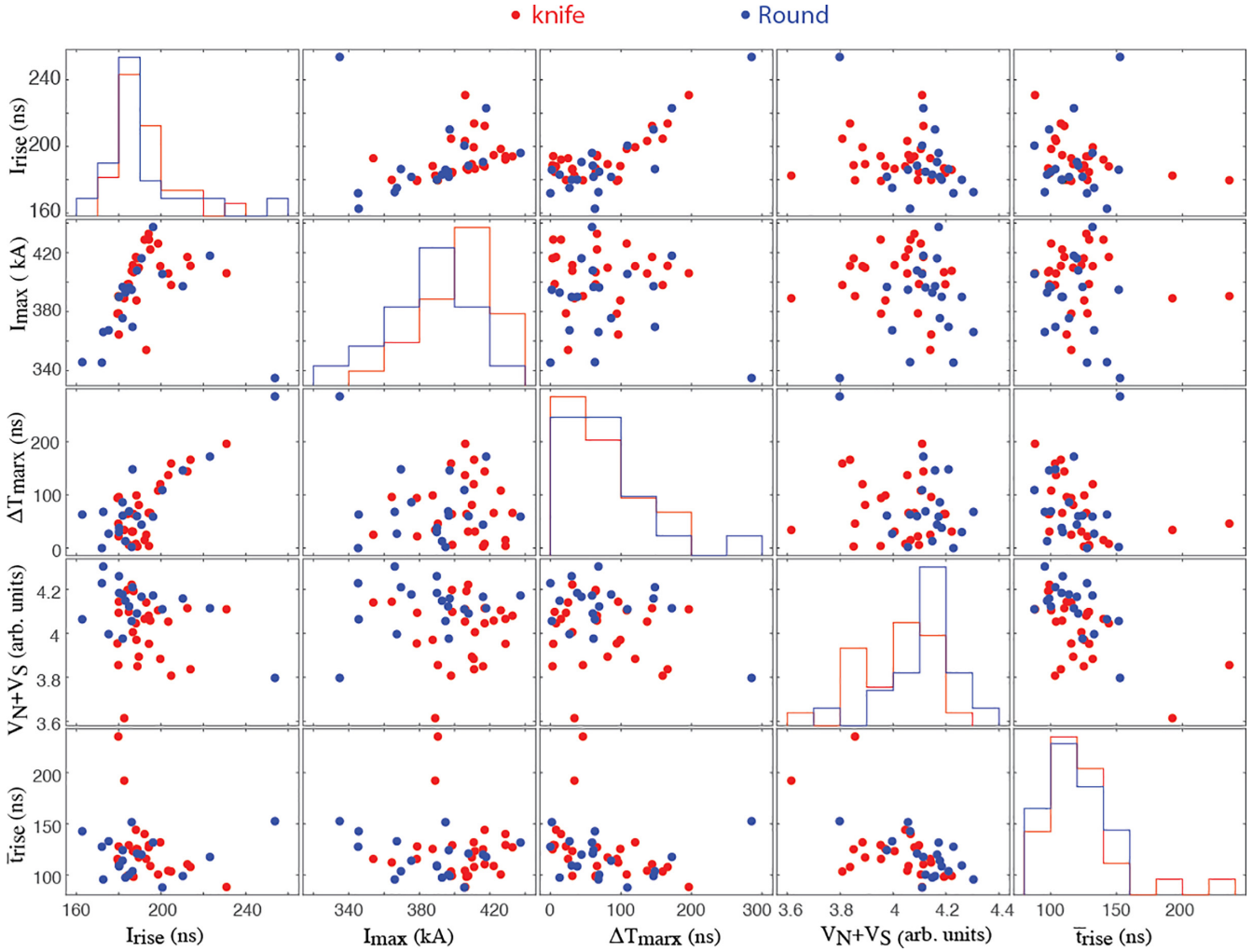


FIG. 7. Correlation plot for the variables defined in Fig. 6. In the diagonal are shown histogram for each variable, while the correlation plots are found off-diagonal.

III. RESULTS AND DISCUSSION

In order to perform a systematic study, we took 19 shots with the round cathode and 26 with the knife cathode. A sample of the collected data is found in Fig. 3 for shot 510 with a round cathode.

From the data we see that pinch time, defined as the moment of most intense x-ray emission, occurs at ~ 300 ns from the current onset [see Fig. 3(b)]. XUV imaging in Fig. 3(a) shows the evolution of the plasma, where fast compression is observed in the last 50 ns of the implosion. During this time MRT grows quickly, inducing a nonuniform compression at stagnation. This is observed in Fig. 3(c), where time-integrated x-ray imaging shows an axially nonuniform source across all the energy bands.

In order to compare the performance of both cathodes, in Fig. 4 we show the x-ray energy yield obtained from the photo-conductive detectors and the time integrated camera. Data is shown in a box plot, the central mark indicates the median, while the left and right edge of the box indicate the 25th

and 75th percentiles, respectively. The whiskers extend to the most extreme data point not considering the outliers, which are plotted individually using the diamond marker symbol.

From the PCD data we observe more emission above 1 keV (Be filter) from the round cathode, although it presents larger dispersion. On the other hand, similar K-shell emission is found for both cathodes. From the pinhole camera, we observe in general more emission from the round cathode, but also with larger dispersion. The image plate/scanner system used to read the films were not calibrated and hence, the use of the PSL (photostimulated luminescence) unit in the pinhole camera results.

The dispersion in the x-ray yield could be due to multiple effects, for example, variations in the current [see Fig. 1(c)] that compresses the plasma and thus producing differences in the final plasma state, or the preionization induced by the cathodes used in this work. To test these options, we plot the peak current data for both cathodes in Fig. 5. From the plot, it can be observed that the median in the round cathode case has a lower value and larger dispersion in contrast to the knife

cathode which has a larger median and smaller dispersion. These results are consistent with the observations made after x-ray yields previously described.

To further test if the differences in the x-ray yield are due to the current dispersion or inherent to preionization and the cathodes, we look for any correlation between driver parameters upstream the load and the current at the load. For example, we want to find out if the larger current seen for the knife cathode is due to the inherent variation of the driver parameters or the cathode itself.

The parameters that could affect the driver performance (i.e., the current through the load) are shown in Fig. 6 and are described as follows: (i) synchronization between the Marxes, north (N) and south (S), defined by the variable Δt_{marx} ; (ii) maximum charge voltage at the main transmission line voltage, given by V_N and V_S ; (iii) voltage rise time at the moment of energy transfer, which depends on the inductance of the SG, defined by $t_{N\text{rise}}$ and $t_{S\text{rise}}$. Figure 6 shows a reference plot for shot 510 and the variables we just defined.

Figure 7 shows a correlation plot where in the diagonal are plotted histograms for each variable. For example, in the second plot in the diagonal we see a comparison for the current for each cathode. From this plot we conclude the same as in Fig. 5, larger current is obtained from the knife cathode and it presents less dispersion than the round one. Off-diagonal plots are the correlation plots. For example, on plot (1,2) and (2,1) we show I_{max} vs I_{rise} ; here we see that the current increases with the rise time, i.e., linear correlation, up to 200 ns after which the current flattens out. We also observe positive correlation between the current rise time and the synchronization between the Marxes (ΔT_{marx}). Nevertheless, we do not see any correlation between the peak current and ΔT_{marx} [see plot (2,3) or (3,2)]. Notice that the time reported in this plot (ΔT_{marx}) is the absolute value of the time difference between the Marxes, as any of them could go earlier than the other. On plot (2,4) and (4,2) we show I_{max} vs $V_N + V_S$. We choose the sum of the voltage because the load current increases linearly with the voltage of each TL. Here, we do not see any correlation between these variables. For the case of the voltage rise time, we choose the average value between both TL, \bar{t}_{rise} , which are shown in plots (2,5) and (5,2). As before, no correlation is observed between these variables. We also do not see correlation between I_{rise} and the Marx voltage or the voltage rise time.

This indicates that the current differences observed in the experiment plotted in Fig. 5 not due to the driver fluctuations but to the cathode themselves. In this case, we conclude that the knife cathode is more reproducible than the round one, although with slightly less yield.

Even though data dispersion is explained by the cathodes, it seems relevant to compare the implosion performance in a similar current range. In this case, we need to find a range where the current overlaps for both cathodes, which we find to be 390–410 kA. In this range we find seven shots overlapping. If we look at the energy yield for these shots in Fig. 8, we still find that the dispersion is smaller for the knife cathode compared to the round one, further supporting the conclusion that the knife cathode is more reproducible. Nevertheless, from the seven shots selected, six had K-shell emission for the round cathode while only three for the knife one. So, even

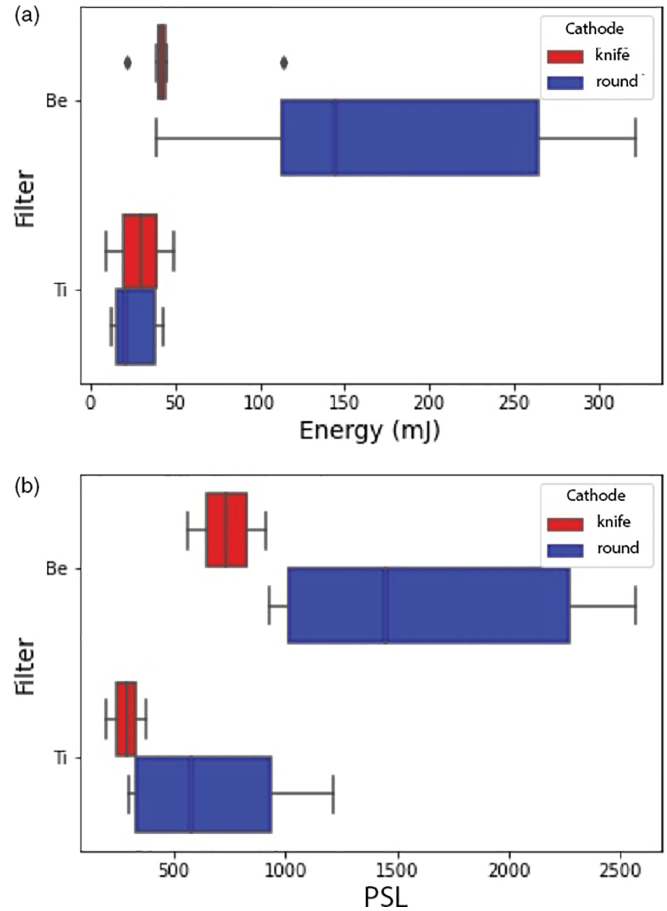


FIG. 8. X-ray yield for the reduced data range 390–410 kA where the current for both cathodes overlap. (a) yield from the photoconductive detectors (b) from the pinhole camera.

if the dispersion is smaller for the knife cathode it is harder to get it to emit in the K-shell range.

We can further compare the implosion dynamics by plotting the average radius found from the XUV imaging as a function of time. Plot 9(a) shows a comparison for both cathodes using all the data obtained from each cathode. Notice that each shot contributes with up to four data points, since our MCP has four independent quadrants triggered at different times for the same shot. We observe the implosion of the plasma given by the reduction in radius in Fig. 9. The plasma compression is described by the snowplow model [16], from where we can find the best curve that fits the experimental data, also plotted in Fig. 9. For the model, we use the density profile found in the CFD simulations, and for the current we used the average trace for each cathode. A series of simulations were run where the density profile were changed slightly by a multiplying factor to produce different implosion curves. Then, we minimized the χ^2 value giving us the best fit. Note that $t = 0$ in the plots corresponds to the pinch time.

Even though the dispersion of data is high and data points for both cathodes seem to overlap, the radii in the knife-edge case are always smaller, indicating earlier implosion when compared to the round case. Moreover, the implosion velocity can be calculated after temporal derivative of the fitted radial curve. This is also shown in Fig. 9(a). We observe that for

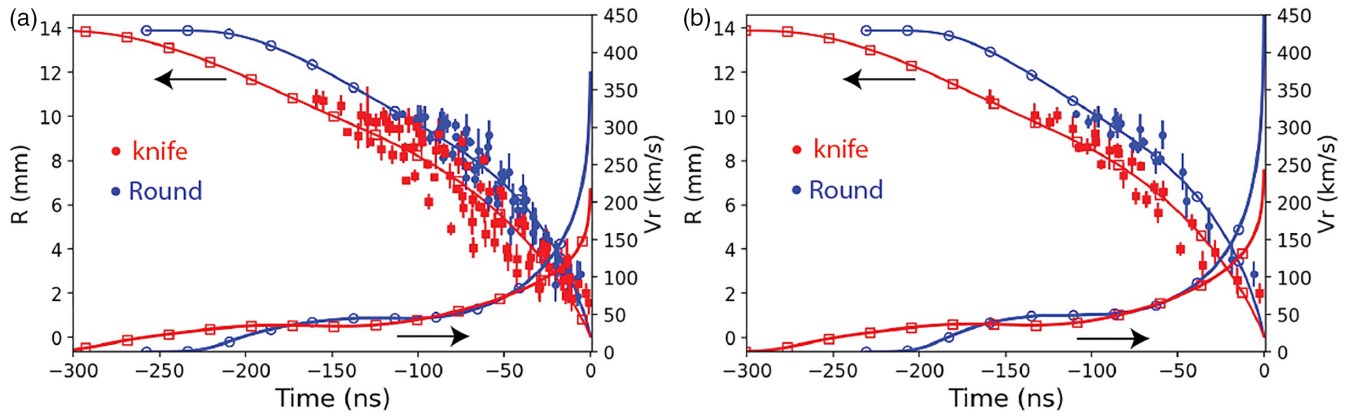


FIG. 9. Average radius vs time obtained from the XUV images. In blue circles the round cathode case is shown while in red squares, the knife cathode. Each shot contributes up to four data points. Solid line shows the best fit from the snowplow model and its first derivative, i.e., implosion velocity. (a) shows the case for all the shots analyzed, while (b) shows only the shots where the current overlaps 390 kA to 410 kA.

the first ~ 70 ns the implosion velocity for the knife cathode is larger than the round one, then the velocity is similar between -200 ns and -50 ns, after which the round cathode accelerates and implodes faster than the knife cathode. Peak velocities reach 200 km/s and 350 km/s for the knife-edge and round cathode, respectively. Similar conclusions are withdrawn if we only consider the shots where peak current overlaps, 390 kA to 410 kA, which is shown in Fig. 9(b). The snowplow model implemented does not take into account the plasma pressure, which means that the final implosion velocities could be overestimated. However, estimations of the ram pressure suggest that it is at least ten times larger than the thermal pressure, indicating that the model is still valid at this time.

The free parameter in the snowplow model is the initial gas load mass. Therefore, after finding the best fit we can calculate necessary mass per unit length to produce that implosion. We find that for the knife cathode it has to be $9 \mu\text{g}/\text{cm} \pm 25\%$ and $3 \mu\text{g}/\text{cm} \pm 30\%$ for the round cathode, while the initial estimated mass load is $15 \mu\text{g}/\text{cm} \pm 50\%$. This tells important information regarding gas preionization and its implosion. First, none of the cathode implodes all the injected mass: the knife cathode implodes $\sim 60\%$ while the round cathode implodes only $\sim 20\%$. Second, the knife cathode works better at coupling the driver current to the load and larger fraction of its mass is imploded compared to the round cathode. Third, this explains the differences in the implosion velocities found. As the round cathode implodes less mass than the knife, it implodes faster.

Finally, the larger velocity found for the round cathode could explain why we observe more shots with K-shell emission compared to the knife cathode.

IV. CONCLUSION

We implemented two cathode geometry, round and knife, to study its effect on the implosion dynamics of a single liner argon gaspuff. No external preionization was used, so current conduction is possible due to self-breakdown.

Self-preionization relies on the electric field distribution between the anode-cathode region so free electrons can accelerate and gain enough energy to ionize a neutral atom. In our case, the round cathode produces a relatively uniform electric field, while the knife cathode produces a larger field locally at the cathode, helping in the production and acceleration of electrons.

Systematic comparison was done over 19 shots for the round cathode and 26 with the knife one. We found that the x-ray yield was more reproducible for the knife cathode, where the round cathode shows a dispersion at least two times larger than the knife one. We also found a larger current (median), and more reproducible, for the knife cathode; again the dispersion for the round one is almost twice as large.

We showed that the current dispersion is due to the cathodes and not to fluctuations in the driver itself. Even if we consider a current range where both cathodes overlap, we still find a better reproducibility for the knife cathode, supporting the argument that the dispersion in the x-ray yield is due to the geometry of the cathodes. Nevertheless, more shots with K-shell emission are observed for the round cathode.

Finally, we observed that the implosion occurs earlier for the knife cathode, but the round cathode accelerates faster during the last 50 ns of the implosion, reaching velocities on the order of 350 km/s compared to 200 km/s for the knife cathode. This difference in velocity could potentially explain the disparities in K-shell emission. According to the snowplow model, only approximately 60% of the total mass is utilized in the compression process for the knife cathode, while only around 20% is used for the round cathode. This highlights the significance of the cathode's geometry in gas-puff experiments, as well as the crucial role of preionization in achieving reliable results.

ACKNOWLEDGMENTS

This research was supported by FONDECYT Grant No. 1220533, FONDECYT Postdoctoral Grant No. 3230401, and QUIMAL Grant No. 190011.

- [1] C. Deeney, P. D. LePell, B. H. Failor, J. S. Meachum, S. Wong, J. W. Thornhill, K. G. Whitney, and M. C. Coulter, Radius and current scaling of argon K-shell radiation, *J. Appl. Phys.* **75**, 2781 (1994).
- [2] H. Sze, J. Banister, B. H. Failor, J. S. Levine, N. Qi, A. L. Velikovich, J. Davis, D. Lojewski, and P. Sincerny, Efficient Radiation Production in Long Implosions of Structured Gas-Puff Z Pinch Loads from Large Initial Radius, *Phys. Rev. Lett.* **95**, 105001 (2005).
- [3] H. U. Rahman, F. J. Wessel, and N. Rostoker, Staged Z-Pinch, *Phys. Rev. Lett.* **74**, 714 (1995).
- [4] C. A. Coverdale, C. Deeney, A. L. Velikovich, R. W. Clark, Y. K. Chong, J. Davis, J. Chittenden, C. L. Ruiz, G. W. Cooper, A. J. Nelson, J. Franklin, P. D. Lepell, J. P. Apruzese, J. Levine, J. Banister, and N. Qi, Neutron production and implosion characteristics of a deuterium gas-puff Z pinch, *Phys. Plasmas* **14**, 022706 (2007).
- [5] J. Shiloh, A. Fisher, and N. Rostoker, Z pinch of a gas jet, *Phys. Rev. Lett.* **40**, 515 (1978).
- [6] M. Krishnan, K. W. Elliott, C. G. R. Geddes, R. A. van Mourik, W. P. Leemans, H. Murphy, and M. Clover, Electromagnetically driven, fast opening and closing gas jet valve, *Phys. Rev. ST Accel. Beams* **14**, 033502 (2011).
- [7] Y. Song, P. Coleman, B. H. Failor, a. Fisher, R. Ingermanson, J. S. Levine, H. Sze, E. Waisman, R. J. Comisso, T. Cochran, J. Davis, B. Moosman, a. L. Velikovich, B. V. Weber, D. Bell, and R. Schneider, Valve and nozzle design for injecting a shell-on-shell gas puff load into a z pinch, *Rev. Sci. Instrum.* **71**, 3080 (2000).
- [8] J. L. Giuliani, J. W. Thornhill, E. Kroupp, D. Osin, Y. Maron, A. Dasgupta, J. P. Apruzese, A. L. Velikovich, Y. K. Chong, A. Starobinets, V. Fisher, Y. Zarnitsky, V. Bernshtam, A. Fisher, T. A. Mehlhorn, and C. Deeney, Effective versus ion thermal temperatures in the Weizmann Ne Z-pinch: Modeling and stagnation physics, *Phys. Plasmas* **21**, 031209 (2014).
- [9] F. J. Wessel, E. Ruskov, H. U. Rahman, P. Ney, T. W. Darling, Z. Johnson, E. McGee, A. Covington, E. Dutra, J. C. Valenzuela, F. Conti, J. Narkis, and F. Beg, Staged Z-pinch Experiments on the University of Nevada, Reno, NTF ZEBRA Facility, in *58th Meet. APS Div. Plasma Physics, San Jose*, 2016.
- [10] M. Krishnan, K. W. Elliott, R. E. Madden, P. L. Coleman, J. R. Thompson, A. Bixler, D. C. Lamppa, J. L. McKenney, T. Strizic, D. Johnson, O. Johns, M. P. Vigil, B. Jones, D. J. Ampleford, M. E. Savage, M. E. Cuneo, and M. C. Jones, Architecture, implementation, and testing of a multiple-shell gas injection system for high current implosions on the Z accelerator, *Rev. Sci. Instrum.* **84**, 063504 (2013).
- [11] E. Ruden, H. U. Rahman, A. Fisher, and N. Rostoker, Stability enhancement of a low initial density hollow gas-puff z pinch by e beam preionization, *J. Appl. Phys.* **61**, 1311 (1987).
- [12] R. S. Smith, III and W. O. Doggett, Experimental characterization of a puff-gas z-pinch plasma prior to implosion, *Appl. Phys. Lett.* **46**, 1128 (1985).
- [13] H. Chuaqui, E. Wyndham, C. Friedli, and M. Favre, LLAM-PÜDKEŇ: A high-current, low-impedance pulser employing an auxiliary exponential transmission line, *Laser Part. Beams* **15**, 241 (1997).
- [14] J. C. Valenzuela, F. Conti, M. P. Ross, N. Aybar, J. Narkis, F. N. Beg, F. J. Wessel, E. Ruskov, H. U. Rahman, P. Ney, T. Darling, A. Covington, D. A. Hammer, T. Byvank, J. T. Banasek, J. B. Greenly, W. M. Potter, and S. V. Rocco, Staged Z-pinch experiments on the Mega-Ampere current driver COBRA, in *44th IEEE International Conference on Plasma Science (ICOPS), Atlantic City, NJ* (IEEE, Piscataway, NJ, 2017).
- [15] F. Conti, J. C. Valenzuela, N. Aybar, F. J. Wessel, M. P. Ross, J. Narkis, H. U. Rahman, E. Ruskov, and F. N. Beg, Characterization of a liner-on-target injector for staged z-pinch experiments, *IEEE Trans. Plasma Sci.* **46**, 3855 (2018).
- [16] J. L. Giuliani and R. J. Comisso, A review of the gas-puff z-pinch as an x-ray and neutron source, *IEEE Trans. Plasma Sci.* **43**, 2385 (2015).